The Astrophysical Journal, 705:1226–1236, 2009 November 10 doi:10.1088/0004-637X/705/2/1226

PLANETS AND DEBRIS DISKS: RESULTS FROM A *SPITZER*/MIPS SEARCH FOR INFRARED EXCESS

G. Bryden[1], C. A. Beichman[2], J. M. Carpenter[3], G. H. Rieke[4], K. R. Stapelfeldt[1], M. W. Werner[1], A. M. Tanner[1,5], S. M. Lawler[2,6], M. C. Wyatt[7], D. E. Trilling[8], K. Y. L. Su[4], M. Blaylock[4], and J. A. Stansberry[4]
[1] Jet Propulsion Lab, California Institute of Technology, 4800 Oak Grove Dr, Pasadena, CA 91109, USA
[2] NASA Exoplanet Science Institute, California Institute of Technology, 770 S Wilson Ave, Pasadena, CA 91125, USA
[3] Department of Astronomy, California Institute of Technology, Mail Code 105-24, 1200 E California Blvd, Pasadena, CA 91125, USA
[4] Steward Observatory, University of Arizona, 933 N Cherry Ave, Tucson, AZ 85721, USA
[5] Department of Physics and Astronomy, Georgia State University, Atlanta, GA 30302, USA
[6] Astronomy Department, Wesleyan University, Middletown, CT 06459, USA
[7] Institute of Astronomy, University of Cambridge, Cambridge, CB3 0HA, UK
[8] Department of Physics and Astronomy, Northern Arizona University, 602 S Humpreys St, Flagstaff, AZ 86011, USA
Received 2007 August 21; accepted 2009 September 16; published 2009 October 20

ABSTRACT

Using the MIPS camera on the *Spitzer Space Telescope*, we have searched for debris disks around 104 stars known from radial velocity studies to have one or more planets. Combining this new data with 42 already published observations of planet-bearing stars, we find that 14 of the 146 systems have IR excess at 24 and/or 70 μm. Only one star, HD 69830, has IR excess exclusively at 24 μm, indicative of warm dust in the inner system analogous to that produced by collisions in the solar system's asteroid belt. For the other 13 stars with IR excess the emission is stronger at 70 μm, consistent with cool dust (<100 K) located beyond 10 AU, well outside of the orbital location of the known planets. Selection effects inhibit detection of faint disks around the planet-bearing stars (e.g., the stars tend to be more distant), resulting in a lower detection rate for IR excess than in a corresponding control sample of nearby stars not known to have planets (9% ± 3% versus 14% ± 3%). Even taking into account the selection bias, we find that the difference between the dust emission around stars with planets and stars without known planets is not statistically significant.

Key words: circumstellar matter – infrared: stars – Kuiper Belt – planetary systems

Online-only material: color figure

1. INTRODUCTION

In addition to its large planets, the Sun is orbited by smaller asteroids, comets, and Kuiper Belt objects—debris left over from the process of planet formation. This debris fills the solar system with dust produced by collisions between these small bodies and, in the case of comets, by sublimation of their surface ices. Though solar radiation removes the dust on timescales much shorter than the Sun's lifetime, ongoing production results in enough dust to be seen with the naked eye—the zodiacal light. The first evidence of similar dust production around other main-sequence stars was provided by the *Infrared Astronomical Satellite* (*IRAS*) detection of IR excess around Vega, a nearby A star (Aumann et al. 1984). Since then, hundreds of stars have been identified as having excess IR emission, many with the *Spitzer Space Telescope* (e.g., Rieke et al. 2005; Su et al. 2006). For solar-type stars, this excess emission is typically detected at 70 μm, corresponding to dust temperatures of ∼30–100 K and orbital distances of tens of AU. Although *Spitzer* is not sensitive enough to detect emission as faint as the solar system's, ∼15% of mature, solar-type stars do have sufficient dust to be detected by *Spitzer* at this wavelength (Trilling et al. 2008; Hillenbrand et al. 2008).

Given the short lifetime of the dust due to inward Poynting–Robertson drag and outward blowout by radiation pressure, extrasolar systems with IR excess must have orbiting populations of dust-producing planetesimals. Some of these systems also have large planets. Usually, planets can only be inferred from the dust distribution; resolved images of debris disks often reveal asymmetries and warps that may be attributed to the gravitational influence of unseen planets (e.g., Wyatt et al. 1999). The most convincing example of planetary influence is the dust ring around the A star Fomalhaut, which is confined to a tight, eccentric orbit that would readily disperse in the absence of some shepherding force (Stapelfeldt et al. 2004; Kalas et al. 2005). Confirming this interaction, the predicted planet has now been directly imaged (Kalas et al. 2008). Further suggesting a link between debris and planets, three planets have been similarly imaged around HR 8799 (Marois et al. 2008), a system with both interior and exterior belts of dust (Sadakane & Nishida 1986; Chen et al. 2006; Su et al. 2009).

Rather than infer the presence of large planets, we consider here systems whose planets are well established by radial-velocity measurements of the central star (e.g., Butler et al. 2006). For such systems, it is not clear what relationship to expect between planets and debris, since the dust responsible for the observed IR emission is generally well exterior to the radial-velocity planets. Still, even without any direct overlap, the inner planets and outer dust must originate from the same protostellar disk. Presumably disks with high surface density at ∼1–10 AU, where the giant planets form, will also tend to have higher density in the outer regions (tens of AU) where the parent bodies of the dust reside. In other words, massive disks that are favorable to forming giant planets (e.g., Ida & Lin 2004) should also be favorable for forming the large quantities of planetesimals throughout the disk that eventually produce bright debris disk emission. Adding a simple prescription for giant planet formation to detailed simulations of debris disk evolution (Wyatt et al. 2007c), for example, Wyatt et al. (2007a) predict that the brightest 10% of debris disks found around planet-bearing A-type stars should tend to be brighter by a factor of ∼6 than the corresponding population around non-planet-

bearing stars (see their Figure 5). While this model applies only to high-mass stars, it implies that a similar type of correlation between planets and dust may exist for solar-type stars.

Another possibility for a dust–planet relationship is that the planetesimals and dust are not connected so much during the planet formation process, but rather through later, more recent events. Observed systems with IR excess are much brighter than the solar system, possibly because they are undergoing a temporary outburst of dust creation. Such an outburst of collisional activity occurred in the solar system ∼0.7 Gyr after the planets formed, as determined by the cratering records of the inner solar system combined with meteoritic and lunar sample dating (see, e.g., Strom et al. 2005). This event, known as the Late Heavy Bombardment, may have been driven by the long-term orbital evolution of our gas giant planets, with an instability occurring as Jupiter and Saturn passed through their 2:1 mean-motion resonance (Gomes et al. 2005). The corresponding dust production would result in strong emission in the *Spitzer* 24 and 70 μm wavebands over hundreds of Myr (Booth et al. 2009). Based on models of resonant planet interaction, Thommes et al. (2008) conclude that similar instabilities resulting in systemwide collisional events may be common in extrasolar planetary systems on timescales comparable to and in some cases longer than the solar system's Late Heavy Bombardment. In support of this conjecture, Wyatt et al. (2007b) find that "hot dust" systems (those with dust inside of 10 AU) around Sun-like stars are inconsistent with either the gradual grinding down of local asteroid belts or from single large collisions. Instead, this hot dust must originate in an outer planetesimal belt which may have been recently perturbed by a dynamical instability in its planetary system. Further evidence for temporary outbursts comes from resolved imaging. The large mass loss inferred to be flowing from Vega's debris disk suggests that this system is undergoing a transient event (Su et al. 2005), the origin of which may also be in the dynamics of its planetary system.

Lastly, planetesimals may be continually stirred via gravitational interaction with an otherwise stable planetary system. In most cases, the observed radial-velocity planets and debris are well separated, with the warm dust system HD 69830 as the exception. The *Spitzer*/IRS spectrum for this star shows detailed spectral features indicative of asteroidal-type dust orbiting at ∼1 AU (Beichman et al. 2005a; Lisse et al. 2007). With three Neptune-mass planets orbiting at 0.08, 0.19, and 0.63 AU (Lovis et al. 2006), the dust may be trapped at the outer planet's 2:1 resonance at 1.0 AU. While such high-order resonances are common between extrasolar planets (Kley et al. 2004), HD 69830 is the only system with radial-velocity planets close enough to the debris for strong mean-motion resonances to play a role in the dust evolution. Secular resonances, however, can be important over greater distances and hence should be more relevant in the cold dust systems considered here. For the HD 38529 system, which contains two planets with $M\sin i$ of 0.8 and 12.2 $M_{\rm Jup}$ at 0.13 and 3.74 AU, Moro-Martín et al. (2007b) find that secular resonances can greatly excite planetesimal orbits at much greater distances than mean-motion resonances, creating a break in the debris at 50–60 AU. This planetary excitation could lead to enhanced planetesimal collision rates and greater dust production.

In order to determine how frequently planet-bearing stars have IR excesses and to help understand the relationship between planets and debris, we have undertaken an infrared survey of planet-bearing stars. Unlike previous far-IR instruments, the MIPS camera on *Spitzer* (Rieke et al. 2004) has the sensitivity to detect the photospheres of nearby ($\lesssim$25 pc) stars, allowing for measurement of relatively faint IR excesses. Preliminary results presented in Beichman et al. (2005b) found that 6 of the 26 observed stars had excess IR emission, the first systems identified as having both well-confirmed planets and dust. While this detection rate was high compared to that for a corresponding non-planet sample (23% versus 10%), the difference was only marginally significant due to the small number of observations. In a related study, Moro-Martín et al. (2007a) observed nine additional planet-bearing stars, finding one with IR excess. Combining their results with 11 planet-bearing stars from Bryden et al. (2006) they did not find any correlation between planets and IR excess, but with such a small sample (20 stars total) only weak constraints could be derived. Similarly, a submillimeter survey for dust emission around planet-bearing stars only observed eight such systems (Greaves et al. 2004).

To understand the relationship between planets and debris disks with greater certainty, a larger sample is needed. Here, we report on the results from our full survey, combined with stars from Moro-Martín et al. (2007a) and other programs, for a total of 146 planet-bearing stars observed with MIPS. After describing the sample selection in Section 2, we present the entire set of MIPS observation in Section 3, determining the dust luminosities for each star with significant IR excess and upper limits for those without. Based on these disk properties, Section 4 compares the planet-bearing stars to a sample of stars not known to have planets, quantifying the observed relationship between dust emission and the presence of planets. We summarize in Section 5.

2. STELLAR SAMPLE

Throughout this paper, we contrast between two samples—stars with known radial-velocity planets and stars without. The bulk of the planet-bearing sample comes from two programs—an initial guaranteed time (GTO) survey with observations from 2004 to 2006 (PI: G. Rieke) and a later general observer (GO) survey from 2007 to 2008 (PI: J. Carpenter). The early dataset consists of 46 planet-bearing stars, 25 already discussed by Beichman et al. (2005b) and 21 newly presented here, while the later data set has 71 additional MIPS observations. The stars in both sets of data were chosen specifically because of their identification as planet bearing. On top of this core group, we include all earlier observations of planet-bearing stars falling within other MIPS surveys such as the FEPS legacy program (Meyer et al. 2004) and the 5 pc GTO survey (Gautier et al. 2007). Overall, 146 planet-bearing stars have been observed, with a total of 184 orbiting planets (some systems are known to have multiple planets). Table 1 lists the basic parameters (spectral type, distance, K band magnitude, and estimated age) for each of these stars, as well as the source program.[9] Note that while the vast majority of planet detections are around solar-type stars, six of the planet-bearing stars with *Spitzer* images are M dwarfs and one is a giant (HD 104985). For consistency between the planet and non-planet samples, most of the discussion below will concentrate on just Sun-like stars (defined here as spectral types F5–K5 and luminosity class IV–V). Similarly, the recently imaged planetary systems around A stars (Kalas et al. 2008; Marois et al. 2008) are not considered here, because their

[9] For completeness, three stars with retracted/unconfirmed planet discoveries are listed in Table 1—HD 33636, HD 150706, and HD 188753A. We do not included these stars in our planet-bearing sample.

Table 1
Spitzer Observations of Planet-Bearing Stars

Star Name		Spectral	Distance	K	Age		F_ν at 24 μm		F_ν at 70 μm		χ_{70}[a]	$L_{\rm dust}/L_\star(70\ \mu{\rm m})$[b]	*Spitzer*
		Type	(pc)	(mag)	(Gyr)	Ref.	(mJy)	$/F_{\nu,*}$	(mJy)	$/F_{\nu,*}$		($\times 10^{-5}$)	Ref.
HD 142[c,d]		F7 V	25.6	4.47	5.4	1, 2, 3	125	1.07	26.7 ± 2.2	2.1	6.0	0.8	1
HD 1237[c]		G6 V	17.6	4.86	0.3	1, 3, 4	84.1	1.03	11.2 ± 2.5	1.3	0.9	<1.0	1
HD 3651	54 Psc	K0 V	11.1	4.00	6.2	1, 5, 6	195	1.08	15.7 ± 5.6	0.8	−0.7	<1.1	2a
HD 4203		G5	77.8	7.05	9.7	5			0.8 ± 8.4	0.7	0.0	<23.9	2b
HD 4208		G5 V	32.7	6.16	5.3	1, 4, 5			3.0 ± 2.6	1.1	0.1	<2.9	2b
HD 4308		G5 V	21.9	4.95	4.0	1	77.3	1.02	4.6 ± 4.4	0.6	−0.8	<1.5	2c
HD 6434		G2/3 V	40.3	6.19	0.2	7	24.5	1.02	4.2 ± 3.8	1.6	0.4	<3.7	3
HD 8574		F8	44.1	5.78	7.9	5	34.9	1.00	2.8 ± 2.2	0.7	−0.4	<1.5	2a
HD 9826[c]	ups And	G0	13.5	2.86	6.7	5, 6	538	1.02	54.8 ± 5.1	1.0	−0.4	<0.3	2a
HD 10647[d,e]		F8 V	17.4	4.34	2.0	2	197	1.38	878.0 ± 13.6	56.7	63.0	42.2	2a
HD 10697	109 Psc	G5	32.6	4.60	8.1	5	102	0.98	1.0 ± 4.7	0.1	−2.1	<1.3	2a
HD 11964[c]		G8 IV	34.0	4.49	9.8	1, 5			3.8 ± 3.8	0.3	−2.2	<1.0	2b
HD 12661		K0	37.2	5.86	8.3	3	32.5	1.00	14.2 ± 7.1	4.0	1.5	<6.5	2d
HD 13445[c]		K1 V	10.9	4.12	2.8	1, 2, 4, 7	166	1.03	5.5 ± 6.8	0.3	−1.7	<1.5	1
HD 16141[c]		G8 IV	35.9	5.27	8.1	3	57.3	1.02	12.8 ± 5.0	2.1	1.3	<2.6	2d
HD 17051	iot Hor	G0 V	17.2	4.14	0.9	1, 2, 3, 4, 7	170	1.07	22.4 ± 3.1	1.3	1.6	<0.5	1
HD 19994[c,d]	94 Cet	G0 V	22.4	3.75	6.2	1, 3, 5, 8	245	1.02	42.5 ± 3.8	1.6	3.9	0.5	2a
HD 20367		G0	27.1	5.04	0.6	5	67.7	0.98	9.3 ± 3.4	1.2	0.5	<1.1	2a
HD 20782[c]		G3 V	36.0	5.83	4.7	1, 2, 4			3.5 ± 2.8	1.0	0.0	<2.1	2b
HD 22049[d,e]	eps Eri	K2 V	3.2	1.78	0.8	9	2040	1.18	1688.0 ± 10.0	9.0	90.9	10.7	4
HD 23079		F8/G0 V	34.6	5.71	5.8	1, 2, 3, 4	37.4	1.00	5.4 ± 1.5	1.3	0.9	<0.9	2a
HD 23127		G2 V	89.1	7.09	6.6	2			−3.0 ± 2.7	−2.6	−1.5	<7.3	2b
HD 23596		F8	52.0	5.87	7.7	5	33.7	1.05	3.3 ± 4.1	0.9	−0.1	<3.1	2a
HD 27442[c]	eps Ret	K2 IV	18.2	1.75	10.9	2, 3	1174	0.98	136.0 ± 5.8	1.0	0.6	<0.3	1
HD 27894		K2 V	42.4	7.07					0.6 ± 2.5	0.5	−0.2	<10.6	2b
HD 28185		G5/6 V	39.6	6.18	6.3	1, 3	23.4	0.97	1.1 ± 4.7	0.4	−0.3	<5.7	2a
HD 30177		G8 V	54.7	6.71	8.1	2			0.9 ± 5.0	0.6	−0.1	<11.2	2b
HD 33283		G3/5 V	86.9	6.65	5.0	13			7.9 ± 3.1	4.6	2.0	<4.9	2b
HD 33564		F7 V	21.0	3.91	5.7	1	196	1.00	24.0 ± 5.0	1.1	0.5	<0.5	2a
HD 33636[d,f]		G1/2 V	28.7	5.57	4.0	1, 3, 5	42.8	1.01	35.4 ± 2.3	7.7	13.4	5.8	1
HD 37124		G0	33.2	5.95	4.8	5			2.8 ± 7.7	0.9	−0.1	<7.2	2b
HD 37605		K0	42.9	6.82					−3.7 ± 8.7	−2.5	−0.6	<23.2	2b
HD 38529[c,d]		G4 IV	42.4	4.21	5.8	5	151	1.02	64.6 ± 6.9	4.0	6.9	3.2	3
HD 39091		G1 V	18.2	4.24	5.3	1, 3, 4	142	0.98	23.4 ± 2.9	1.5	2.5	<0.5	1
HD 39091		G1 V	18.2	4.24	5.3	1, 3, 4	142	0.98	23.4 ± 2.9	1.5	2.5	<0.5	3
HD 40307		K3 V	12.8	4.79	7.3	1	89.8	1.04	17.9 ± 4.8	1.9	1.8	<2.3	2c
HD 40979[c]		F8	33.3	5.45	1.4	5	48.4	1.02	14.0 ± 3.5	2.7	2.5	<1.6	2a
HD 41004A[c]		K1 V	43.0	6.43	1.6	4			3.9 ± 3.7	1.9	0.5	<6.9	2b
HD 45350		G5	49.0	6.22	8.4	5			−0.9 ± 5.5	−0.3	−0.6	<7.2	2b
HD 46375[c]		K0 V	33.4	6.00	6.9	1, 5			316.6 ± 194.5	102.2	1.6	<252.3	2b
HD 49674		G0	40.7	6.43	3.2	5			3.8 ± 2.9	1.8	0.6	<4.5	2b
HD 50499		G0/2 V	47.3	5.84	7.4	4, 5			7.5 ± 2.9	2.1	1.3	<2.2	2b
HD 50554[d]		F8	31.0	5.47	5.7	3	47.6	1.02	42.4 ± 3.8	8.4	9.7	6.0	1
HD 52265[d]		G0 V	28.1	4.95	6.4	3, 5	75.1	1.00	38.3 ± 5.7	4.7	5.3	3.0	1
HD 63454		K4 V	35.8	7.00	0.7	1			−0.3 ± 4.0	−0.2	−0.4	<16.0	2b
HD 65216[c]		G5 V	35.6	6.33	5.1	1			4.7 ± 3.3	2.1	0.7	<4.4	2b
HD 66428		G8 IV	55.0	6.66	8.1	5			1.8 ± 5.7	1.1	0.0	<10.7	2b
HD 68988		G0	58.8	6.74	7.4	5			1.5 ± 2.3	1.0	0.0	<4.2	2b
HD 69830[e]		K0 V	12.6	4.17	6.0	1, 5	238	1.54	15.3 ± 2.3	0.9	−0.6	<0.5	5
HD 70642		G8/K1	28.8	5.57	5.2	1, 2			−9.7 ± 9.1	−2.1	−1.6	<6.3	2b
HD 72659		G2 V	51.4	5.98	7.0	5			6.7 ± 2.6	2.1	1.4	<2.2	2b
HD 73256		G8/K0 V	36.5	6.26	1.0	1, 4			2.4 ± 3.8	1.0	0.0	<5.5	2b
HD 73526		G6 V	94.6	7.30	7.5	2			41.3 ± 16.2	44.2	2.5	<56.0	2b
HD 74156		G1 V	64.6	6.21	8.1	5			−3.2 ± 3.5	−1.2	−1.6	<3.4	2b
HD 75289[c]		G0 V	28.9	5.01	6.7	1, 4			−28.8 ± 46.2	−3.7	−0.8	<14.9	2b
HD 75732[c]	55 Cnc	K0 IV-V	12.5	4.01	7.2	1, 5, 6	175	0.99	20.9 ± 4.2	1.1	0.4	<0.9	1
HD 76700		G6 V	59.7	6.50	9.1	2			2.2 ± 2.2	1.1	0.1	<3.7	2b
HD 81040		G0	32.6	6.16					5.9 ± 2.9	2.2	1.1	<3.2	2b
HD 82943[d]		G2/3 V	27.5	5.11	4.8	1, 3, 5	67.8	1.04	119.4 ± 4.4	16.9	25.5	14.6	1
HD 83443		K0/1 V	43.5	6.44	3.8	5			−3.5 ± 5.0	−1.7	−1.1	<9.0	2b
HD 89307		G0	30.9	5.56	5.7	5			−1.0 ± 5.1	−0.2	−1.1	<2.8	2b
HD 89744[c]		F8 IV	39.0	4.45	7.2	3, 6	117	0.99	11.6 ± 5.3	0.9	−0.2	<0.9	2d
HD 92788		G6 V	32.3	5.72	5.9	5	35.6	0.96	2.6 ± 5.6	0.6	−0.3	<4.4	3

Table 1
(Continued)

Star Name		Spectral	Distance	K	Age		F_ν at 24 μm		F_ν at 70 μm		χ_{70}[a]	$L_{\rm dust}/L_\star$(70 μm)[b]	*Spitzer*
		Type	(pc)	(mag)	(Gyr)	Ref.	(mJy)	$/F_{\nu,*}$	(mJy)	$/F_{\nu,*}$		($\times 10^{-5}$)	Ref.
HD 93083		K3 V	28.9	6.13	8.1	1			7.9 ± 5.7	2.9	0.9	<9.2	2b
HD 95128	47 UMa	G0	14.1	3.75	6.4	5, 6, 8	272	1.05	31.7 ± 3.6	1.1	0.9	<0.4	1
HD 99492[c]		K2/4	18.0	5.26	5.5	3	58.8	1.04	7.5 ± 6.3	1.2	0.2	<5.1	2c
HD 101930[c]		K1 V	30.5	6.15	8.4	1			−5.9 ± 9.4	−2.2	−0.9	<14.8	2b
HD 102117		G6 V	42.0	5.83	7.2	2			−6.0 ± 18.2	−1.7	−0.5	<16.8	2b
HD 102195		K0 V	29.0	6.15	0.1	10			3.8 ± 6.6	1.4	0.2	<9.2	2b
HD 104985		G9 III	102.0	3.27	9.5	3	358	1.03	37.3 ± 4.5	1.0	−0.1	<0.4	2a
HD 106252		G0	37.4	5.93	6.0	5	30.4	1.00	10.6 ± 5.2	3.2	1.4	<4.2	3
HD 107148		G5 V	51.3	6.47	7.2	5			−11.4 ± 3.6	−5.7	−3.7	<5.6	2b
HD 108147		F8/G0 V	38.6	5.72	0.6	10			5.4 ± 41.9	1.4	0.0	<23.9	2b
HD 108874		G5	68.5	7.06	8.1	5			4.7 ± 4.7	4.0	0.8	<13.6	2b
HD 109749[c]		G3 V	59.0	6.68					−3.0 ± 3.6	−1.8	−1.3	<6.2	2b
HD 111232		G8 V	28.9	5.90	7.1	1, 4			−0.7 ± 6.8	−0.2	−0.6	<6.1	2b
HD 114386		K3 V	28.0	6.35	6.5	1			6.2 ± 3.0	2.8	1.3	<6.8	2b
HD 114729[c]		G0 V	35.0	5.14	7.2	1, 3, 4, 5	63.9	1.01	10.0 ± 2.6	1.5	1.2	<1.0	2a
HD 114762[c]		F8	40.6	5.81	11.8	3	33.0	0.97	−1.3 ± 5.6	−0.4	−0.9	<3.3	2d
HD 114783		K1 V	20.4	5.47	6.1	1, 3	46.0	0.99	6.5 ± 3.6	1.3	0.4	<3.0	1
HD 117176[d]	70 Vir	G0	18.1	3.50	8.8	5, 6, 8	380	0.99	72.1 ± 4.1	1.7	6.0	0.8	1
HD 117207		G8 IV/V	33.0	5.65	7.3	1, 4, 5			4.0 ± 2.8	0.9	−0.1	<2.1	2b
HD 117618		G2 V	38.0	5.74	5.0	1, 4			−0.8 ± 3.5	−0.2	−1.3	<2.3	2b
HD 118203		K0	88.6	6.54	8.0	11			8.9 ± 8.2	4.7	0.9	<13.2	2b
HD 120136[c]	tau Boo	F5	15.6	3.51	0.6	5, 7, 8	345	1.10	33.5 ± 6.4	1.0	−0.1	<0.4	1
HD 121504		G2 V	44.4	6.12	1.9	3, 4	25.7	1.01	35.7 ± 17.4	12.9	1.9	<16.3	3
HD 128311[d]		K3 V	16.6	5.14	0.4	1, 7	61.0	0.97	21.0 ± 3.2	3.1	4.4	3.2	1
HD 130322		K0 V	29.8	6.23	1.0	3	24.3	1.06	4.7 ± 5.6	1.9	0.4	<7.9	2d
HD 134987	23 Lib	G5 V	25.6	4.88	7.5	1, 3, 4, 5	77.9	0.97	3.5 ± 7.3	0.4	−0.7	<2.6	1
HD 136118		F7 V	52.3	5.60	6.0	5	39.5	0.96	2.9 ± 2.5	0.6	−0.6	<1.3	2a
HD 141937		G2/3 V	33.5	5.76	5.1	5	34.4	0.97	3.0 ± 8.1	0.8	−0.1	<5.6	3
HD 142022A[c]		G9 IV-V	35.9	5.96	8.9	1, 4			7.5 ± 3.6	2.3	1.2	<3.8	2b
HD 142415		G1 V	34.6	5.89	1.8	1, 2, 4			−1.0 ± 13.6	−0.3	−0.3	<10.9	2b
HD 143761	rho CrB	G0 V	17.4	3.86	4.5	1, 5, 6, 7, 8	204	0.99	31.4 ± 5.4	1.4	1.6	<0.6	1
HD 145675	14 Her	K0 IV-V	18.1	4.71	8.1	1, 5, 6	93.9	1.01	10.5 ± 2.5	1.0	0.2	<1.0	1
HD 147513[c]		G3/5 V	12.9	3.93	0.4	3	205	1.07	18.4 ± 12.2	0.9	−0.2	<1.6	6
HD 149026		G0	78.9	6.82					2.3 ± 2.8	1.6	0.3	<5.2	2b
HD 149143		G3 V	63.5	6.43	6.0	12			5.6 ± 3.3	2.7	1.1	<4.6	2b
HD 150706[d,g]		G0	27.2	5.57	2.0	5	46.0	1.08	39.2 ± 9.1	8.5	3.8	6.5	3
HD 154345		G0	18.1	5.00	5.0	5	70.5	0.99	4.5 ± 4.4	0.6	−0.7	<1.9	2c
HD 154857		G5 V	68.5	5.51	7.9	2, 4, 11			0.0 ± 7.5	0.0	−0.6	<4.7	2b
HD 159868		G5 V	52.7	5.54	7.1	2, 4			−18.5 ± 14.9	−3.9	−1.6	<9.9	2b
HD 160691	mu Ara	G3 IV/V	15.3	3.68	7.5	1, 3, 4	274	1.03	30.7 ± 7.8	1.1	0.2	<0.9	1
HD 162020		K2 V	31.3	6.54	0.3	1			−25.7 ± 11.8	−13.6	−2.3	<28.6	2b
HD 164922		G9 V	21.9	5.11	9.1	1	62.7	0.97	11.0 ± 6.3	1.6	0.6	<3.3	2c
HD 168443		G6 V	37.9	5.21	8.3	1, 3, 5	57.6	0.98	8.9 ± 29.1	1.4	0.1	<14.7	1
HD 168746		G5 V	43.1	6.25	7.5	5			92.0 ± 344.7	37.5	0.3	<444.9	2b
HD 169830		F8 V	36.3	4.69	6.8	1, 2, 3, 5	100	1.05	9.6 ± 7.1	0.9	−0.1	<1.5	1
HD 177830[c]		K0	59.0	4.81	11.2	3	89.7	1.05	6.1 ± 3.2	0.7	−1.0	<1.4	1
HD 178911B[c]		G5	46.7	6.38	6.2	5			5.0 ± 5.5	2.3	0.5	<8.4	2b
HD 179949		F8 V	27.1	4.94	2.9	5	74.3	0.98	−9.2 ± 7.0	−1.1	−2.5	<1.9	3
HD 183263		G5	52.8	6.42	8.6	5			11.4 ± 6.8	5.4	1.4	<9.1	2b
HD 185269		G0	47.4	5.26	5.0	12			4.8 ± 5.6	0.8	−0.2	<2.4	2b
HD 186427[c]	16 Cyg B	G3 V	21.4	4.65	7.4	1, 5, 8	96.5	0.98	−1.4 ± 4.7	−0.1	−2.6	<1.3	1
HD 187085		G0 V	45.0	5.88	5.3	4			11.8 ± 3.2	3.4	2.5	<2.3	2b
HD 187123		G5	47.9	6.34	7.2	5			1.1 ± 8.4	0.5	−0.1	<10.6	2b
HD 188015[c]		G5	52.6	6.63	7.5	5			19.3 ± 16.0	11.2	1.1	<29.4	2b
HD 188753A[h]		K0	44.8	5.53					−2.8 ± 11.7	−0.6	−0.6	<8.7	2b
HD 189733[c]		K2 V	19.2	5.54	0.9	1, 9	45.4	1.04	5.8 ± 6.1	1.2	0.2	<5.5	2b
HD 190228		G5	62.1	5.35	8.7	5	53.2	1.03	33.8 ± 22.2	6.0	1.3	<14.1	3
HD 190360[c]		G7 IV-V	15.9	4.08	8.0	1, 5			−11.7 ± 55.8	−0.6	−0.5	<9.7	2b
HD 192263[d]		K1/2 V	19.9	5.54	0.4	3	43.8	1.00	22.3 ± 5.0	4.7	3.5	5.4	7
HD 192699		G8 IV	67.4	4.37	2.0	12			14.6 ± 4.6	1.0	0.1	<1.1	2b
HD 195019[c]		G5	37.4	5.26	8.3	5			17.1 ± 4.4	2.8	2.5	<2.1	2b
HD 196050[c]		G3 V	46.9	6.03	7.4	4	28.6	1.03	1.8 ± 2.7	0.6	−0.4	<2.7	2a
HD 196885[c]		F8	33.0	5.07	8.4	3	67.6	1.01	6.0 ± 3.0	0.8	−0.4	<1.0	8

Table 1
(Continued)

Star Name		Spectral	Distance	K	Age		F_ν at 24 μm		F_ν at 70 μm		χ_{70}[a]	$L_{\rm dust}/L_\star(70\ \mu{\rm m})$[b]	*Spitzer*
		Type	(pc)	(mag)	(Gyr)	Ref.	(mJy)	$/F_{\nu,*}$	(mJy)	$/F_{\nu,*}$		($\times 10^{-5}$)	Ref.
HD 202206[d]		G6 V	46.3	6.49	2.2	3			28.9 ± 3.1	14.6	8.6	14.3	2b
HD 208487		G1/3 V	44.0	6.16	4.8	4			−2.3 ± 5.6	−0.8	−0.9	<4.9	2b
HD 209458		F8	47.1	6.31	5.7	3	21.6	1.00	−10.2 ± 3.9	−4.4	−3.2	<4.2	2d
HD 210277		G8/K0 V	21.3	4.80	7.9	1, 3, 5	85.1	0.99	8.3 ± 2.2	0.9	−0.5	<0.8	1
HD 212301[c]		F8 V	52.7	6.47					3.5 ± 4.2	1.7	0.4	<4.9	2b
HD 213240[c]		G0/1 V	40.8	5.35	6.3	3, 4	50.5	0.98	6.8 ± 2.3	1.2	0.5	<1.1	2a
HD 216435[d]		G0 V	33.3	4.61	7.2	1, 3, 4			39.1 ± 3.6	3.5	7.6	2.2	2b
HD 216437	rho Ind	G2/3 IV	26.5	4.52	9.0	1, 2, 3	110	0.98	7.1 ± 5.1	0.6	−1.0	<1.4	1
HD 216770		K0 V	37.9	6.31	4.7	1, 3, 5			8.9 ± 11.6	3.8	0.6	<19.0	2b
HD 217014	51 Peg	G3 V	15.4	3.91	7.3	1, 4, 5, 8	193	0.99	26.7 ± 4.5	1.3	1.2	<0.7	2a
HD 217107		G8 IV/V	19.7	4.54	8.1	3	112	1.02	10.9 ± 5.3	0.9	−0.2	<1.5	2d
HD 222404[c]	gam Cep	K1 IV	13.8	1.04	11.1	3	3635	1.03	355.3 ± 5.4	0.9	−1.0	<0.3	2a
HD 222582[c]		G5 V	42.0	6.17	7.2	3	24.3	1.00	8.3 ± 2.2	3.1	2.6	<2.3	2a
HD 224693		G2 V	94.1	6.81	5.0	12			7.1 ± 4.1	4.8	1.4	<8.0	2b
HD 330075		G5	50.2	7.17	7.2	3			8.4 ± 22.3	8.0	0.3	<67.0	2b
BD-10 3166		K0 V		8.12	5.1	3	3.6	0.90	−9.1 ± 4.6	−20.9	−2.1	<39.8	2d
HIP 14810		G5	52.9	6.83					−4.6 ± 4.7	−3.2	−1.3	<10.9	2b
GJ 436		M3 V	10.2	6.07	10.1	3	39.6	0.99	4.8 ± 2.2	1.1	0.2	<6.7	6
GJ 581		M2.5 V	6.3	5.84	1.0	10			15.9 ± 4.7	2.9	2.2	<12.6	2b
GJ 674		M2+ V	4.5	4.86	0.2	10	127	1.03	31.6 ± 16.4	2.4	1.1	<16.9	9
GJ 832		M2/3 V	4.9	4.50	8.4	2	170	1.00	19.2 ± 4.3	1.0	0.2	<2.7	9
GJ 849		M3 V	8.8	5.59	0.6	10			3.8 ± 5.6	0.6	−0.5	<12.3	2b
GJ 876		M3.5 V	4.7	5.01	9.6	3	112	1.05	9.5 ± 3.1	0.8	−0.7	<4.8	9

Notes. Color corrections have not been applied. For cold emission (∼50 K), the color-corrected 70 μm flux is as much as ∼10% higher. Spectral Types from NStED. Distances from the *Hipparcos* satellite. *K* band magnitudes from 2MASS.

[a] Significance of excess (Equation (1)).

[b] Minimum $L_{\rm dust}/L_\star$ based solely on the 70 μm emission (Equation (2)).

[c] Binary or triple star; see Mugrauer & Neuhäuser (2009) for individual references.

[d] Star with excess 70 μm emission.

[e] Star with excess 24 μm emission

[f] Based on the *Hubble Space Telescope* (*HST*) astrometry, Bean et al. (2007) conclude that the companion of HD 33636 is not a planet but rather a low-mass star in a near face-on orbit. While Beichman et al. (2005b) identified HD 33636 as a planet-bearing star with strong 70 μm excess, we no longer include this star in our planet sample.

[g] Radial-velocity observations by Moro-Martín et al. (2007a) and Wright et al. (2007) do not confirm the planet around HD 150706. This star is not included in our sample.

[h] Radial-velocity observations by Eggenberger et al. (2007) do not confirm the planet around HD 188753A. This star is not included in our sample.

References. *Spitzer* data references: (1) Beichman et al. 2005b; (2) This paper; (2a) from *Spitzer* PID 41, PI: G. Rieke; (2b) PID 40096, PI J. Carpenter; (2c) PID 30590, PI D. Koerner; (2d) PID 72, PI F. Low; (3) Moro-Martín et al. 2007a; (4) Backman et al. 2009; (5) Beichman et al. 2005a; (6) Beichman et al. 2006a; (7) Smith et al. 2006 (8) Trilling et al. 2007; (9) Gautier et al. 2007.

References. Age references: (1) Gray et al. 2003, 2006; (2) Jenkins et al. 2006, 2008; (3) Saffe et al. 2005; (4) Henry et al. 1996; (5) Wright et al. 2004; (6) Soderblom 1985; (7) Barnes 2007; (8) Hall et al. 2007; (9) Backman et al. 2009; (10) Montes et al. 2001b; (11) Butler et al. 2006; (12) This paper.

planet-detection technique has different selection biases and because the sample of such systems is too small for meaningful statistical analysis.

As a separate but related *Spitzer* GTO project, we have completed a survey of solar-type stars for IR excess (Bryden et al. 2006; Trilling et al. 2008). This sample contains 108 nearby F5–K5 stars not known to have planets. Chosen primarily based on the expected signal-to-noise ratio (S/N) for their stellar photospheres, this sample represents most of the brightest Sun-like stars in the sky. Unlike the planet-bearing stars, however, the targets were pre-screened to exclude regions with a high degree of infrared cirrus contamination, as expected from *IRAS* images. The original GTO sample is extended here by a second survey for debris disks that focused on potential Space Interferometry Mission (SIM) and Terrestrial Planet Finder (TPF) target stars (Beichman et al. 2006a). These targets are again nearby stars chosen with the same selection algorithm (e.g. pre-screening with *IRAS*), but covering a wider range of spectral types (F0–M5). For our solar-type star control sample, we include only the 57 stars in that survey with spectral types F5–K5. Our overall non-planet sample then contains a total of 165 solar-type stars.

The planet and non-planet samples are both biased against the inclusion of binary stars to some extent. For both optical radial-velocity planet searches and infrared debris disk surveys, some screening is done to maximize the success rate—a companion star orbiting at several AU is assumed to rule out the presence of a planet or disk at a similar location. Nevertheless, despite efforts to cull such systems, there are stars in both sets of data that do in fact have low-mass stellar companions (the multiple-star systems in our planet sample are indicated in Table 1). For the radial-velocity surveys, these are typically wide binaries discovered as follow-up after the planet detection (e.g., Mugrauer et al. 2005; Chauvin et al. 2006). While some of the non-planet stars are also now known to be binaries, they generally have not been monitored for companions as

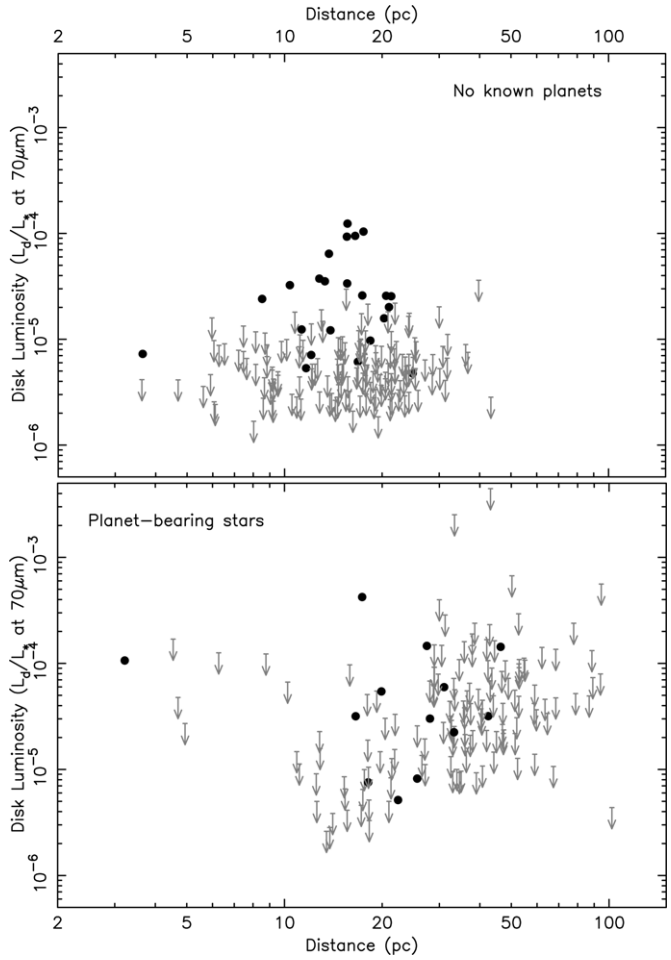

Figure 1. Debris disk fractional luminosities for stars without known planets (upper panel) and for stars with planets (lower panel) as a function of stellar distance. For stars with significant excess (solid points), a minimum $L_{\rm dust}/L_\star$ is derived from the strength of the 70 μm emission relative to the stellar photosphere (Equation (2)). Otherwise, 3σ upper limits are shown, again based solely on the 70 μm emission. (Note that the planet-bearing star HD 69830 has a large 24 μm excess, but for self-consistency its $L_{\rm dust}/L_\star$ is shown here as an upper limit based solely on its 70 μm emission.) Overall, the planet-bearing stars tend to be farther away and have not been limited to clean regions of the sky, making it more difficult to detect faint emission around them.

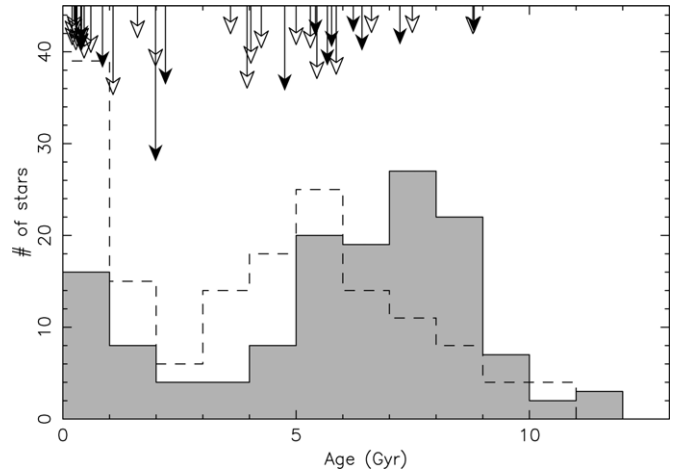

Figure 2. Estimated ages for the observed stars. The ages for the planet-bearing stars are shown as a filled histogram, while those for the control sample of stars not known to have planets are outlined with a dashed line. The ages of stars with 70 μm excess are flagged as arrows at the top of the plot, with the length of each arrow proportional to the strength of the excess emission. Solid arrows indicate IR excess stars known to have planets while open arrows correspond to stars in the control sample.

closely as the planet stars. Overall, since similar binary selection methods have been applied to both samples, they should contain a similar fraction of low-mass, long-period stellar companions. Neither sample has been modified a posteriori to remove wide-separation binaries.

It is intended that the only inherent difference between the two types of stars is whether or not they are known to have planets. Selection effects that might unintentionally contribute to different rates of IR excess between the two samples must be considered in detail. For example, while stars in the control sample mostly range from 5 to 30 pc away, the planet-bearing stars tend to be considerably more distant and hence fainter (see Figure 1, lower panel). Differences in data quality due to variations in stellar fluxes and image background noise have been explicitly taken into account below by considering not just the stars with detections but also those with upper limits (Section 4.2).

An additional factor to consider is stellar age. The age sampling can potentially bias an IR excess survey, since younger stars are more likely to have circumstellar dust (e.g., Rieke et al. 2005; Siegler et al. 2007). While the trend with age is relatively weak for the old stars considered here (e.g., Bryden et al. 2006; Trilling et al. 2008), it is still necessary to rule out any age bias that might exist between the two samples. Age determinations in the literature, however, utilize a range of methods and calibrations. Quoted values can have very poor accuracy and may be inconsistent from one reference to another. To put the age estimates for our two samples of stars on a homogeneous scale, we have compiled a set of age estimates with uniform assumptions. Most of these ages are based on chromospheric activity, for which we adopted the calibration of Mamajek & Hillenbrand (2008); they quote an uncertainty of 0.2 dex. Their calibration is largely based on young stars. To verify its application to older ones, we constructed a Hertzsprung-Russell diagram in M_K versus $V-K$ for stars with parallaxes determined to 3% or better. Much of the scatter on this diagram is due to metallicity differences. We used the metallicity-dependent isochrones of An et al. (2007) to develop a transformation that, to first order, compensates for the shifts in the positions in our HR diagram with metallicity. After applying this transform to our sample of stars, we then compared the ages from the extrapolated chromospheric activity relation of Mamajek & Hillenbrand (2008) with the isochrones from the Padova group (these isochrones are similar to those of An et al. for ages in common but extend to older ages). The agreement for ages greater than 5 Gyr is excellent, with good correspondence between the methods in distinguishing stars differing by 2 Gyr in age. For younger ages the isochrones are too similar to provide useful age discrimination. This procedure validates the activity-index age calibration for old stars to the accuracy needed for our work. In a few cases, we also considered ages determined by gyrochronology (Barnes 2007; Reiners & Schmitt 2003) and, with lower weight, moving-group membership (Montes et al. 2001b, 2001a). The net results of this age compilation are given in Table 1, along with the related references. Figure 2 plots the resulting age distribution for the planet-bearing sample (filled histogram) along with the distribution for the non-planet sample (dotted line). The median ages are 6.4 Gyr for the stars with planets and 4.2 Gyr for those not known to have planets. Neither sample was chosen based on stellar age, but

the planet-bearing stars are somewhat older than a random sample of nearby stars since radial-velocity measurements can more easily detect planetary oscillations around lower activity (i.e., older) stars. This age bias can potentially decrease the likelihood of finding IR excesses around the older planet-bearing stars and might weaken our ability to detect a positive correlation between planets and debris. We find below, however, that the overall effect is not large, with no qualitative change in the overall results when the youngest stars (<1 Gyr) are excluded.

Finally we stress that the phrase "non-planet" throughout this paper is shorthand for systems that are not yet known to have orbiting planets. While all of the stars in our sample have been targeted by radial-velocity surveys looking for planets, these surveys are only sensitive to relatively massive planets. Cumming et al. (2008) conclude, for example, that nearly all Jupiter-mass planets within ∼3 AU of their parent star and Saturn-mass planets within ∼0.5 AU have now been identified within their Keck Planet Search data. Planets with lower masses or longer periods almost certainly exist around many of the stars in our so-called non-planet sample. The distinguishing factor between the two samples is the presence of a gas giant planet on a short to moderate period orbit.

3. *SPITZER* OBSERVATIONS

Previous *Spitzer* surveys have found that 70 μm is the optimal wavelength for identifying IR excess around mature solar-type stars, with detection rates ∼5 times higher than at 24 μm (Bryden et al. 2006; Trilling et al. 2008). The focus below is on 70 μm; all stars in both our planet and non-planet samples have been observed by *Spitzer*'s MIPS camera at this wavelength. Most stars were concurrently observed by MIPS at 24 μm, with the exception of 71 planet-bearing stars from *Spitzer* program PID 40096 (indicated in the final column of Table 1). These stars were instead observed by *Spitzer*'s intensified Reticon spectograph (IRS) from 8 to 35 μm. Only the MIPS photometry is presented here; see S. Dodson-Robinson et al. (2009, in preparation) for analysis of the IRS spectra.

Overall, our data analysis is similar to that previously described in Beichman et al. (2005b), Bryden et al. (2006), and Beichman et al. (2006a). At 24 μm, images are created from the raw data using software developed by the MIPS instrument team (Gordon et al. 2005), with image flats chosen as a function of scan mirror position to correct for dust spots and with individual frames normalized to remove large-scale gradients (Engelbracht et al. 2007). At 70 μm, images are also processed with the MIPS instrument team pipeline, including added corrections for time-dependent transients (Gordon et al. 2007). Aperture photometry is performed as in Beichman et al. (2005b) with aperture radii of 15.″3 and 14.″8, background annuli of 30.″6–43.″4 and 39.″4–78.″8, and aperture corrections of 1.15 and 1.79 at 24 and 70 μm, respectively. The 24 μm centroid positions, which are consistent with the telescope pointing accuracy of <1″ (Werner et al. 2004), are used as the target coordinates for both wavelengths. Three images require special attention. One star, HD 23596, has a patch of 70 μm emission located ∼15″ to the north which overlaps the target aperture, such that dual-point-spread function (PSF) fitting must be used to disentangle the two distinct sources. Similarly, the 24 μm image of HD 189733 contains two faint sources ∼10″ and 15″ away; removing the emission from these background contaminants via triple-PSF fitting lowers the measured target flux by ∼10%. For another star, HD 142, we mask out an IR-bright point source located ∼2′ north of the target. While this mask does not alter the flux within the aperture, it does decrease the noise measured within the image background. As a final comment on the data reduction we note that since previous papers were published (e.g., Beichman et al. 2005b), improvements in the instrument calibration have increased the overall 70 μm flux conversion by 4% from 15.8 to 16.5 mJy arcsec^{-2}/MIPS_70_unit (MIPS_70_unit is an internally defined standard based on the ratio of the measured signal to that from the stimulator flash signal; Gordon et al. 2007).

For the planet-bearing stars, the MIPS flux and background noise measurements are listed in Table 1, while those from the non-planet sample are reported in Bryden et al. (2006), Beichman et al. (2006a), and Trilling et al. (2008). All of the stars observed at 24 μm have high S/N; uncertainty at that wavelength is dominated by systematics at the level of ∼2% for overall calibration, <1% for repeatability (Engelbracht et al. 2007), and ∼4% for predicting the stellar photosphere (Beichman et al. 2006a). At 70 μm, targets in the non-planet sample are generally bright enough for their stellar photospheres to also be detected at this wavelength. Most such systems—135 of 165—are observed with S/N greater than 3. The detection rate is much lower for the planet-bearing stars (just 41 of 146 have S/N > 3) due to their greater distances and, in some cases, noisier backgrounds. Note that the 70 μm uncertainties listed in Table 1 are from direct measurement of the background variation in each field. A systematic repeatability uncertainty of ∼4.5% (Gordon et al. 2007) is also included when determining the significance of any excess.

The first step in looking for excess is predicting each star's photospheric emission in the absence of any orbiting dust. For most stars, the easiest and most accurate method is a simple extrapolation from 2MASS K band out to longer wavelengths. For this extrapolation, we use MIPS zero points of 7.17 and 0.778 Jy at 24 and 70 μm, respectively (Rieke et al. 2008). Two groups of stars require more detailed modeling. First, some stars in our sample (those with $K \lesssim 4$ mag) are bright enough to saturate their Two Micron All Sky Survey (2MASS) images. Instead of relying on these stars' poor near-IR measurements, optical photometric data are compiled from the literature and fit to Kurucz stellar atmosphere models (for details see the appendix of Bryden et al. (2006)). The second issue is that using the standard zero points for extrapolation assumes that the stars have zero $K-[24]$ color. While this is true for solar-type stars, which are used extensively in the zeropoint calibration, near-IR features in M star atmospheres result in $K-[24]$ colors that range from ∼0.4 to more than 1 mag redder for the latest spectral types, as predicted by Phoenix stellar models (Brott & Hauschildt 2005) and as observed by *Spitzer* (Gautier et al. 2007). For the six late-type stars in our planet sample (types from M2 to M3.5), we set $K-[24] = 0.5$ mag for the stellar photosphere, consistent with the atmospheric models and earlier *Spitzer* observations.

Table 1 lists the observed fluxes relative to the expected stellar fluxes ($F_\nu/F_{\nu,*}$) at 24 and 70 μm. Most fluxes at 24 μm are close to photospheric ($F_\nu = F_{\nu,*}$). Three stars have excess emission at 24 μm: HD 10647, HD 22049 (ϵ Eri), and HD 69830 with $F_\nu/F_{\nu,*} = 1.38$, 1.18, and 1.54, respectively. The remaining sample of stars with 24 μm observations has a mean $F_\nu/F_{\nu,*}$ of 1.01 with a dispersion of 4%. This dispersion is somewhat lower than in the control sample, which has a greater number of bright stars whose 2MASS photometry is saturated. For both samples, we use $F_\nu/F_{\nu,*} >= 1.15$ as a 3σ threshold for detection of significant 24 μm emission. Only one star in the non-planet

sample meets this criterion - HD 166 with $F_\nu/F_{\nu,*} = 1.15$. For the 71 planet-bearing stars without 24 μm photometry, we rely on their IRS spectra as a measure of warm dust emission. With systematic uncertainty of ~2% (e.g., Lawler et al. 2009), these spectra provide tight constraints on excess at 24 μm, such that emission greater than our $F_\nu/F_{\nu,*} = 1.15$ threshold can be excluded (S. Dodson-Robinson et al. 2009, in preparation).

While the dispersion in $F_\nu/F_{\nu,*}$ at 24 μm is dominated by systematics, at 70 μm the background fluctuations due to detector noise and sky variation are more important. For each image, this background noise is directly measured from the variation within the surrounding field after convolving with our chosen photometry aperture and multiplying by the corresponding aperture correction. Adding in systematic calibration uncertainties gives a total noise estimate for each 70 μm target, σ_{70}. The significance of any deviation from the expected level of photospheric emission is then defined as

$$\chi_{70} \equiv \frac{F_{70} - F_{70,\star}}{\sigma_{70}}, \quad (1)$$

where F_{70} is the measured flux and $F_{70,\star}$ is the expected stellar flux, both at 70 μm. χ_{70} greater than 3 indicates significant IR excess. Based on this criterion, we find that 13 out of the 146 planet-bearing stars have a 3σ or greater excess at 70 μm. Four of these IR excesses—HD 142, HD 19994, HD 202206, HD 216435—are newly identified here, while the remainder have been already reported in the literature (see Table 1 for a full list of χ_{70} values and related references). Applying the same analysis to the sample of stars not known to have planets, 23 out of 165 have excess 70 μm emission, all of which have been previously reported elsewhere (e.g., Trilling et al. 2008).

The majority of the excesses detected at 70 μm have corroborating excess within their IRS spectra at ~30 μm (HD 10647 (Chen et al. 2006; Lawler et al. 2009), HD 22049 (Backman et al. 2009), HD 38529 (Moro-Martín et al. 2007a; Carpenter et al. 2009), HD 50554, HD 52265, HD 82943, HD 202206, HD 216435 (S. Dodson-Robinson et al. 2009, in preparation)). The remainder (HD 142, HD 19994, HD 117176, HD 128311, HD 192263) are relatively weak detections at 70 μm (the median dust flux is just two times that expected from the stellar photosphere, as opposed to nine times the photosphere for the IRS excess detections) making detection at shorter wavelengths difficult (e.g., Beichman et al. 2006b). We note that one star, GJ 581, has 70 μm emission three times that expected from its stellar photosphere and has corresponding indications of excess in its IRS spectrum. Due to the faintness of this target, however, the 70 μm excess is only significant at a 2.2σ level, well below our strict 3σ cutoff.

For each detection of excess at 70 μm, we can estimate the dust luminosity by assuming that the emission peaks at the observed wavelengths or, equivalently, by setting the dust temperature to ~50 K. This gives a minimum fractional disk luminosity of

$$\frac{L_{\rm dust}}{L_\star}({\rm minimum}) = 10^{-5} \left(\frac{5600\ {\rm K}}{T_\star}\right)^3 \frac{F_{70,{\rm dust}}}{F_{70,\star}}, \quad (2)$$

where $T_\star$ is the effective temperature of the star. For the 13 planet-bearing stars with 70 μm excess, $L_{\rm dust}/L_\star$ ranges from 5×10^{-6} to 4×10^{-4}, values ~10–1000 larger than estimates for the solar system (10^{-7}–10^{-6} for the Kuiper Belt region beyond 10 AU; Stern 1996). Measured values of $L_{\rm dust}/L_\star$ range from 5×10^{-6} to 1.2×10^{-4} within the non-planet sample. Minimum values of $L_{\rm dust}/L_\star$ are listed in Table 1 for the stars with excess; otherwise 3σ upper limits on the cold dust emission are calculated based on Equation (2). Figure 1 shows these measurements and upper limits as a function of stellar distance for the planet-bearing stars (lower panel) and for the control sample (upper panel). Of particular note, the upper limits for the planet-bearing stars tend to be considerably higher due to their farther distance (a median of 34 pc, compared to 17 pc for the non-planet sample) as well as their occasional location in cirrus-contaminated parts of the sky. Because of this lower sensitivity, the detection of IR excesses is more difficult around the planet-bearing stars, an important effect that must be taken into account in the following section.

4. THE RELATIONSHIP BETWEEN PLANETS AND DUST

In this section, we examine (1) whether the detection frequency of IR excess is correlated with the presence of planets, (2) whether the dust luminosity is correlated with planets, (3) how much larger the dust luminosity might be for planet-bearing stars, (4) how IR excess depends on planet characteristics, and (5) how it depends on stellar metallicity. For consistency, only main-sequence stars of types F5–K5 are considered here in the planet-bearing and non-planet-bearing samples (six M stars and one giant are excluded from the planet sample).

4.1. Correlation of Planets with IR Excess Detection

The most straightforward test for a correlation between planets and debris disks is to check whether planet-bearing stars have a higher frequency of IR excess. While our preliminary results (Beichman et al. 2005b) found a weak (1σ) correlation, the additional data presented here do not support the original trend. The overall detection rate for planet-bearing stars is now lower than for the non-planet stars, though the difference is still not statistically significant (9% ± 3% versus 14% ± 3% for the full sample or 8% ± 3% versus 11% ± 3% when stars younger than 1 Gyr are excluded). IR excesses are not detected significantly more frequently around the planet-bearing stars.

While the frequency of IR excess around planet-bearing stars has decreased since earlier publication, this is primarily due to the most recent targets' farther distances and/or noisier IR backgrounds. To account for this in rough fashion, it is worth considering the detection rates just for the brightest disks. Dust disks with luminosities greater than 10^{-4} $L_\star$ are relatively rare in the non-planet sample—just two out of 165 stars (1.2%) have disks this bright. Every star in the non-planet sample was observed with enough sensitivity to detect a disk this bright. In the planet sample, only 113 of the 139 FGK stars were observed deep enough to detect a disk with $L_{\rm dust}/L_\star = 10^{-4}$. Nevertheless, four of the planet-bearing stars have such bright disks (3.5%). While this rate is higher than in the non-planet sample, the small numbers limit the statistical significance of the difference (see Table 2 for a summary of the detection statistics).

The observations at 24 μm have a similar trend between the strength of IR excess and the presence of planets. Due to the lower contrast relative to the hot stellar emission, 24 μm emission from warm dust is more difficult to detect than at 70 μm. In the non-planet sample, only one star in 165 exhibits a 24 μm excess (HD 166, with $F_\nu/F_{\nu,*} = 1.15$). In contrast with this low-detection rate within the control sample, three planet-bearing stars have 24 μm excess, out of 78 observed at this wavelength. Two of these detections, HD 10647 and ϵ Eri, are not at all surprising based on their 70 μm emission—their

Table 2
Summary of Detection Statistics at 70 μm

Metric	Stars Without Known Planets	Stars With Known Planets[a]
Detection of significant IR excess	23/165 (14% ± 3%)	13/139 (9% ± 3%)
Detection of strong excess ($L_{dust}/L_\star > 10^{-4}$)	2/165 (1.2% ± 0.9%)	4/113[b] (3.5% ± 1.7%)

Notes.
[a] For consistency, only solar-type stars (F5–K5) are considered.
[b] Only 113 of the 139 solar-type stars with planets were observed with sufficient S/N to detect a disk with fractional luminosity of 10^{-4}.

70 μm excesses are the most significant among any stars in either sample, such that significant IR excess at 24 μm can be expected even if the systems are dominated by cold (~50 K) dust. Note, however, that resolved imaging of ϵ Eri reveals a warmer inner dust belt at 24 μm, distinct from the outer 70 μm component (Backman et al. 2009). Only one star, HD 69830, has IR excess exclusively from warm dust in the inner system, analogous to that produced by collisions in the solar system's asteroid belt. Overall, the detection rate for excess at 24 μm, whether it arises from warm or cold dust, is nominally higher for planet-bearing stars (4% ± 2% versus 0.6% ± 0.6% for the planet and non-planet samples), but again suffering from small number statistics.

4.2. Correlation of Planets with Dust Luminosity

Here, we further investigate the possibility that the excess detection rates for the planet and non-planet samples are affected by selection bias. We consider the hypothesis that only relatively bright disks can be detected around the more distant planet-bearing stars (see Figure 1). In order to quantify the impact of this effect, statistical methods that can accommodate upper limits must be employed. Standard survival analysis (Feigelson & Nelson 1985) is specifically designed to handle censored data, and can be implemented using readily available software (ASURV; Lavalley et al. 1992). Several tests are commonly used for determining whether two samples come from the same underlying distribution—Gehan, logrank, and Peto & Prentice. Peto & Prentice is the best choice for the data considered here, in which the two samples have very different censoring (the upper limits tend to be much higher for the planet-bearing stars). Using this method, we find a 77% confidence level for the planet and non-planet samples to have different distribution of $L_{dust}/L_\star$. (The Gehan and logrank tests give confidence levels of 69% and 78% respectively.) *We conclude that there is not a statistically significant correlation between inner planets and IR excess, even when selection biases are considered.*

4.3. Dust Luminosity Distribution

The previous section focused solely on whether or not stars with planets tend to have brighter dust emission than those without, but failed to give a quantitative measure of how much brighter. Here, we calculate the distribution of $L_{dust}/L_\star$ directly from the data, following Bryden et al. (2006). Figure 3 shows how frequently we detect dust emission over a range of detection thresholds measured in terms of $L_{dust}/L_\star$. For each disk brightness level ($L_{dust}/L_\star$), we tabulate how many observations could potentially detect such a disk and how many were actually detected. For example, four out of

Table 3
Summary of Tests for Differences Between the Planet & Non-planet $L_{dust}/L_\star$ Distributions

Metric		Confidence Level
Generic survival analysis	Gehan:	69%
	logrank:	78%
	Peto–Prentice:	77%
Model-specific Monte Carlo simulations	log–linear:	64%
	Gaussian:	59%

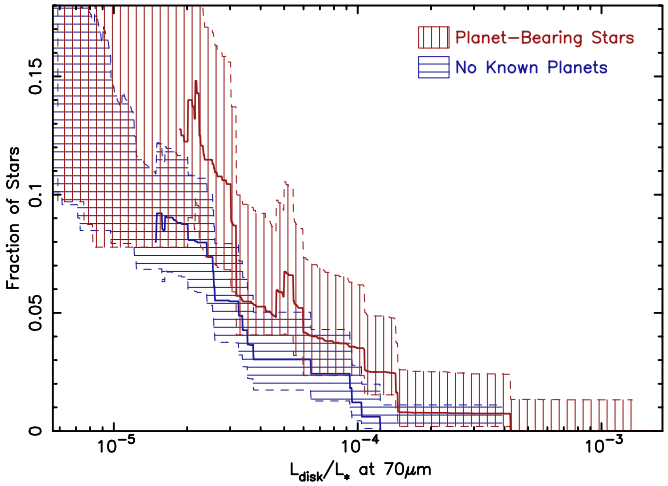

Figure 3. Cumulative fraction of stars with 70 μm excess as a function of disk luminosity for the planet and non-planet samples. As in Figure 1, the dust's fractional luminosity, $L_{dust}/L_\star$, is derived from the strength of the 70 μm emission relative to the stellar photosphere (Equation (2)). For both the planet and non-planet samples, dust disks with $L_{dust}/L_\star > 10^{-4}$ are rare, with $L_{dust}/L_\star \approx 10^{-5}$ disks detected much more frequently. The 1σ uncertainties in the underlying distributions of $L_{dust}/L_\star$ are indicated by the shaded regions. While the dust around planet-bearing stars is nominally brighter than for the non-planet stars (i.e., the red line lies above the blue line), the difference is not statistically significant.
(A color version of this figure is available in the online journal.)

139 solar-type planet-bearing stars are detected with $L_{dust}/L_\star$ greater than 10^{-4}. The background noise in 26 of the images, however, is too high to detect such a disk, such that the overall detection rate is 4/(139−26) = 3.5% for this $L_{dust}/L_\star$. (The individual $L_{dust}/L_\star$ detections and upper limits are all listed in Table 1.) The uncertainties in the underlying distribution (shaded regions in the figure) are based on binomial sampling statistics. The $L_{dust}/L_\star$ distributions are not shown below ~10^{-5}, where measurements of the detection rates are unreliable due to systematic effects. Note that while the true cumulative distribution of $L_{dust}/L_\star$ has to be monotonic, the observed distribution can fluctuate as the statistical sampling varies from point to point. This is in contrast with a traditional cumulative distribution function, which does not take into account the observational limitations of the data set and only rises toward fainter disks.

The $L_{dust}/L_\star$ distribution for planet-bearing stars is shown separately from that for stars with no known planets (the red and blue lines, respectively). There is an offset between the two, with planet-bearing stars tending to have stronger dust emission. To quantify the difference between the two samples, some assumptions have to be made for the unknown shape of the underlying $L_{dust}/L_\star$ distribution. Bryden et al. (2006), for example, considered the possibility that all stars have disks which span a log-normal distribution of luminosities, finding

a best fit to their data centered on a median luminosity of $L_{\rm dust}/L_\star = 10^{-6.5}$, i.e., similar to that expected for the solar system. Here, we consider two possible functional forms for the $L_{\rm dust}/L_\star$ distribution and we find that our data are consistent with either a log-normal distribution or with a simple linear fit to the results in Figure 3. Regardless of the chosen functional form, the best fits to the observed $L_{\rm dust}/L_\star$ distributions in Figure 3 have the planet-bearing stars with ∼1.8 times as much dust emission as stars without any known planets. In other words, the separation between the two lines is a factor of 1.8.

Next we consider the significance of this offset. The generic, non-parametric nature of the survival analysis in the previous section has some advantages; it can be implemented for a wide range of physical applications with results that are easily reproduced. It is possible, however, to improve upon these tests by developing a test that incorporates all relevant information from this specific data set. The errors on the detections, for example, are not taken into account by the survival analysis, which assumes that the measured values of disk luminosity are exact. A parametric analysis of the disk detections, however, requires some assumption for the underlying luminosity distribution. In order to further assess the significance of any difference between the planet and non-planet samples, we have run Monte Carlo simulations under the assumption that the underlying $L_{\rm dust}/L_\star$ distribution follows a Gaussian or a log–linear relationship. For each star in our survey, the disk luminosity is set randomly based on one of these assumed distributions. Using the actual observed background noise in each field to determine which disks would be detectable, we then simulate detection rates for the planet and non-planet stars and determine how much offset there is between their $L_{\rm dust}/L_\star$ distributions. For the log–linear distribution, we find that an offset as large as seen in the real data is found in the simulated data for 36% of the simulations. (A positive correlation as large as observed is found 17% of the time.) For the Gaussian assumed distribution, we expect to find an offset as large as observed 41% of the time. So there is again no evidence for a correlation between RV planets and debris emission, with confidence levels even lower than found by the non-parametric survival tests discussed in the previous section (see Table 3).

4.4. Correlation with Planet Characteristics

Beichman et al. (2005b) did not find any strong correlations between IR excess and planetary characteristics, but did note that no systems with short-period planets (<0.4 AU) were identified with excess. There are now three exceptions to this trend, however, HD 38529, HD 69830, and HD 192263 (HD 38529 also has a massive, $> 13 M_{\rm Jup}$ planet at 3.7 AU). Overall, there is no significant correlation between IR excess and either planet mass or semimajor axis; Kolmogorov–Smirnov (KS) tests find confidence levels of only 45% and 68% that the IR excess stars have different distributions in planet mass or semimajor axis, respectively.

4.5. Correlation with Metallicity

A strong relationship has been observed between planets and their host star's metallicity (e.g., Gonzalez 1997; Santos et al. 2001), with the probability of harboring a radial-velocity detected planet increasing as metallicity squared ($10^{2[{\rm Fe/H}]}$; Fischer & Valenti 2005). However, the detection of IR excess by *IRAS* or the *Infrared Space Observatory* (Greaves et al. 2006) or by *Spitzer* surveys (Bryden et al. 2006; Beichman et al. 2006a) does not appear to be correlated with stellar metallicity. A correlation as strong as that between planets and metallicity can be confidently ruled out.

Previous surveys for IR excess contained relatively few high-metallicity and/or planet-bearing stars. Yet even within our much larger sample of planet stars, there is still no measurable correlation of metallicity with either the detection of IR excess or the strength of IR excess. (This is true both within the planet-bearing sample and when combined with the non-planet sample.) Given the lack of a significant correlation between planets and $L_{\rm dust}/L_\star$ (Section 4.2), it is perhaps not surprising that a second-order correlation with metallicity is also not found. While only a limited constraint is provided here, the lack of a strong trend with metallicity provides evidence against any theory in which the strength of debris disk emission is directly proportional to the solid mass contained within the parent protostellar disk.

5. SUMMARY

A search for debris disks with *Spitzer*'s MIPS far-IR camera has been conducted for 146 stars with known radial-velocity planets. We find that 13 of these stars display excess 70 μm emission, indicating the presence of dust orbiting at Kuiper Belt-like distances in those systems. Three stars have excess emission at 24 μm. While two of the three have stronger emission at 70 μm (eps Eri and HD 10647), HD 69830 does not have significant excess at 70 μm and is instead dominated by warm dust emission at 24 μm. Overall, 14 of 146 planet-bearing stars are found to have 3σ significant excess IR emission at some wavelength (13 at 70 μm, plus HD 69830 at only 24 μm).

Considering only solar-type stars (defined here as spectral types ranging from F5 to K5), we find that 13 out of 139 planet-bearing stars are found to have significant 70 μm excess, compared to 23 out of 165 in a sample of stars not known to have any planets. While the detection rate is lower for the planet sample (9% ± 3% versus 14% ± 3%; see Table 2), there are strong selection effects against the detection of IR excesses around the planet-bearing stars. The control sample is chosen based on stellar brightness, with stars at typical distances of 5–30 pc, while the planet sample contains stars that are often much fainter, located as far away as 100 pc. So although the detection rate is lower for the planet-bearing stars, the debris disks detected around them appear to be brighter than those in the control sample. Fitting the $L_{\rm dust}/L_\star$ distributions, the IR emission from planet-bearing stars is nominally brighter than from stars with no known planets, by a factor of ∼2 (Figure 3). Based on survival statistics, however, this difference between $L_{\rm dust}/L_\star$ for planet-bearing and non-planet stars is not statistically significant (only 77% confidence). Monte Carlo simulations of the observations find even less significance to this possible correlation between planets and disks (59%–64% confidence, depending on the assumed underlying distribution of $L_{\rm dust}/L_\star$).

While we do not find a significant correlation between planets and orbiting dust, we cannot rule out a relationship below our measuremental uncertainty. Debris disks around planet-bearing stars might still be a few times brighter than for those without radial-velocity planets. Further quantification of theoretical models is necessary to compare directly with the observations and additional data are needed to reduce the observational uncertainties. Toward this goal, two Key Projects of the *Herschel Space Observatory*—DUNES (PI: C. Eiroa)

and DEBRIS (PI: B. Matthews)—are dedicated to finding IR excess around hundreds of nearby stars at levels fainter than possible with *Spitzer* and at longer wavelengths, allowing for detection of colder dust. The combined data set from *Spitzer* and *Herschel* will provide tighter constraints on the relationship between planets and dust, or lack thereof.

This paper makes use of data products from the NASA/IPAC/NExScI Star & Exoplanet Database (NStED), the Two-Micron All Sky Survey (2MASS), the NASA/IPAC Infrared Science Archive (IRSA), the SIMBAD and VIZIER databases operated at CDS Strasbourg, the Extrasolar Planets Encyclopaedia, and the California & Carnegie Planet Search website. The *Spitzer Space Telescope* is operated by the Jet Propulsion Laboratory, California Institute of Technology, under NASA contract 1407. This work was partially supported by contract 1255094 from JPL/CalTech to the University of Arizona. Some of the research described in this publication was carried out at the Jet Propulsion Laboratory, California Institute of Technology, under a contract with the National Aeronautics and Space Administration.

REFERENCES

An, D., et al. 2007, ApJ, 655, 233
Aumann, H. H., et al. 1984, ApJ, 278, L23
Backman, D., et al. 2009, ApJ, 690, 1522
Barnes, S. A. 2007, ApJ, 669, 1167
Bean, J. L., et al. 2007, AJ, 134, 749
Beichman, C. A., et al. 2005a, ApJ, 626, 1061
Beichman, C. A., et al. 2005b, ApJ, 622, 1160
Beichman, C. A., et al. 2006a, ApJ, 652, 1674
Beichman, C. A., et al. 2006b, ApJ, 639, 1166
Booth, M., Wyatt, M. C., Morbidelli, A., Moro-Martín, A., & Levison, H. F. 2009, MNRAS, 1141
Brott, I., & Hauschildt, P. H. 2005, in The Three-Dimensional Universe with *Gaia*, ed. C. Turon, K. S. O'Flaherty, & M. A. C. Perryman (ESA SP-576; Noordwijk: ESA), 565
Bryden, G., et al. 2006, ApJ, 636, 1098
Butler, R. P., et al. 2006, ApJ, 646, 505
Carpenter, J. M., et al. 2009, ApJS, 181, 197
Chauvin, G., et al. 2006, A&A, 456, 1165
Chen, C. H., et al. 2006, ApJS, 166, 351
Cumming, A., et al. 2008, PASP, 120, 531
Eggenberger, A., Udry, S., Mazeh, T., Segal, Y., & Mayor, M. 2007, A&A, 466, 1179
Engelbracht, C. W., et al. 2007, PASP, 119, 994
Feigelson, E. D., & Nelson, P. I. 1985, ApJ, 293, 192
Fischer, D. A., & Valenti, J. 2005, ApJ, 622, 1102
Gautier, T. N., III, et al. 2007, ApJ, 667, 527
Gomes, R., Levison, H. F., Tsiganis, K., & Morbidelli, A. 2005, Nature, 435, 466
Gonzalez, G. 1997, MNRAS, 285, 403
Gordon, K. D., et al. 2005, PASP, 117, 503
Gordon, K. D., et al. 2007, PASP, 119, 1019
Gray, R. O., Corbally, C. J., Garrison, R. F., McFadden, M. T., & Robinson, P. E. 2003, AJ, 126, 2048
Gray, R. O., et al. 2006, AJ, 132, 161
Greaves, J. S., Fischer, D. A., & Wyatt, M. C. 2006, MNRAS, 366, 283
Greaves, J. S., Holland, W. S., Jayawardhana, R., Wyatt, M. C., & Dent, W. R. F. 2004, MNRAS, 348, 1097
Hall, J. C., Lockwood, G. W., & Skiff, B. A. 2007, AJ, 133, 862
Henry, T. J., Soderblom, D. R., Donahue, R. A., & Baliunas, S. L. 1996, AJ, 111, 439
Hillenbrand, L. A., et al. 2008, ApJ, 677, 630
Ida, S., & Lin, D. N. C. 2004, ApJ, 604, 388
Jenkins, J. S., et al. 2006, MNRAS, 372, 163
Jenkins, J. S., et al. 2008, A&A, 485, 571
Kalas, P., Graham, J. R., & Clampin, M. 2005, Nature, 435, 1067
Kalas, P., et al. 2008, Science, 322, 1345
Kley, W., Peitz, J., & Bryden, G. 2004, A&A, 414, 735
Lavalley, M., Isobe, T., & Feigelson, E. 1992, in ASP Conf. Ser. 25, Astronomical Data Analysis Software and Systems I, ed. D. M. Worrall, C. Biemesderfer, & J. Barnes (San Francisco, CA: ASP), 245
Lawler, S. M., et al. 2009, ApJ, 705, 89
Lisse, C. M., Beichman, C. A., Bryden, G., & Wyatt, M. C. 2007, ApJ, 658, 584
Lovis, C., et al. 2006, Nature, 441, 305
Mamajek, E. E., & Hillenbrand, L. A. 2008, ApJ, 687, 1264
Marois, C., et al. 2008, Science, 322, 1348
Meyer, M. R., et al. 2004, ApJS, 154, 422
Montes, D., López-Santiago, J., Fernández-Figueroa, M. J., & Gálvez, M. C. 2001a, A&A, 379, 976
Montes, D., et al. 2001b, MNRAS, 328, 45
Moro-Martín, A., et al. 2007a, ApJ, 658, 1312
Moro-Martín, A., et al. 2007b, ApJ, 668, 1165
Mugrauer, M., & Neuhäuser, R. 2009, A&A, 494, 373
Mugrauer, M., Neuhäuser, R., Seifahrt, A., Mazeh, T., & Guenther, E. 2005, A&A, 440, 1051
Reiners, A., & Schmitt, J. H. M. M. 2003, A&A, 412, 813
Rieke, G. H., et al. 2004, ApJS, 154, 25
Rieke, G. H., et al. 2005, ApJ, 620, 1010
Rieke, G. H., et al. 2008, AJ, 135, 2245
Sadakane, K., & Nishida, M. 1986, PASP, 98, 685
Saffe, C., Gómez, M., & Chavero, C. 2005, A&A, 443, 609
Santos, N. C., Israelian, G., & Mayor, M. 2001, A&A, 373, 1019
Siegler, N., et al. 2007, ApJ, 654, 580
Smith, P. S., et al. 2006, ApJ, 644, L125
Soderblom, D. R. 1985, AJ, 90, 2103
Stapelfeldt, K. R., et al. 2004, ApJS, 154, 458
Stern, S. A. 1996, A&A, 310, 999
Strom, R. G., Malhotra, R., Ito, T., Yoshida, F., & Kring, D. A. 2005, Science, 309, 1847
Su, K. Y. L., et al. 2005, ApJ, 628, 487
Su, K. Y. L., et al. 2006, ApJ, 653, 675
Su, K. Y. L., et al. 2009, ApJ, 705, 314
Thommes, E. W., Bryden, G., Wu, Y., & Rasio, F. A. 2008, ApJ, 675, 1538
Trilling, D. E., et al. 2007, ApJ, 658, 1289
Trilling, D. E., et al. 2008, ApJ, 674, 1086
Werner, M. W., et al. 2004, ApJS, 154, 1
Wright, J. T., Marcy, G. W., Butler, R. P., & Vogt, S. S. 2004, ApJS, 152, 261
Wright, J. T., et al. 2007, ApJ, 657, 533
Wyatt, M. C., et al. 1999, ApJ, 527, 918
Wyatt, M. C., Clarke, C. J., & Greaves, J. S. 2007a, MNRAS, 380, 1737
Wyatt, M. C., et al. 2007b, ApJ, 658, 569
Wyatt, M. C., et al. 2007c, ApJ, 663, 365